RSC Advances

PAPER

View Article Online
View Journal | View Issue



Cite this: *RSC Adv.*, 2024, **14**, 9848

# Preparation and properties of a 3D printed nHA/PLA bone tissue engineering scaffold loaded with a β-CD–CHX combined dECM hydrogel

Shangbo Li,[ab] Zijian Liu,[ab] Xiaohan Gao,[ab] Lidi Cheng,[ab] Zexian Xu,[ab] Li Li,[ab] Yaru Diao,[ab] Liqiang Chen,[abc] Yanshan Liu*[abc] and Jian Sun*[abc]

Jaw defects, which can result from a multitude of causes, significantly affect the physical well-being and psychological health of patients. The repair of these infected defects presents a formidable challenge in the clinical and research fields, owing to their intricate and diverse nature. This study aims to develop a personalized bone tissue engineering scaffold that synergistically offers antibacterial and osteogenic properties for treating infected maxillary defects. This study engineered a novel temperature-sensitive, sustained-release hydrogel by amalgamating β-cyclodextrin (β-CD) with chlorhexidine (CHX) and a decellularized extracellular matrix (dECM). This hydrogel was further integrated with a polylactic acid (PLA)–nano hydroxyapatite (nHA) scaffold, fabricated through 3D printing, to form a multifaceted composite scaffold (nHA/PLA/dECM/β-CD–CHX). Drug release assays revealed that this composite scaffold ensures prolonged and sustained release. Bacteriological studies confirmed that the β-CD–CHX loaded scaffold exhibits persistent antibacterial efficacy, thus effectively inhibiting bacterial growth. Moreover, the scaffold demonstrated robust mechanical strength. Cellular assays validated its superior biocompatibility, attributed to dECM and nHA components, significantly enhancing the proliferation, adhesion, and osteogenic differentiation of osteogenic precursor cells (MC3T3-E1). Consequently, the nHA/PLA/dECM/β-CD–CHX composite scaffold, synthesized *via* 3D printing technology, shows promise in inducing bone regeneration, preventing infection, and facilitating the repair of jaw defects, positioning itself as a potential breakthrough in bone tissue engineering.

Received 10th January 2024
Accepted 12th March 2024

DOI: 10.1039/d4ra00261j

rsc.li/rsc-advances



## 1. Introduction

In recent years, jaw defects arising from trauma,[1] infection,[2] tumor,[3] and congenital malformation[4] have emerged as significant concerns impacting people's physical and psychological health. Addressing large jaw defects remains a formidable challenge for clinicians.[5] Presently, common approaches for rectifying these defects include titanium plate implantation, autologous bone grafts, and distraction osteogenesis. Yet, these methods face several limitations, such as mechanical incompatibility with bone tissues, extensive surgical trauma, and heightened infection risks, often leading to suboptimal reconstructive outcomes.[6–8] As research in bone tissue engineering continues to advance, an increasing body of evidence suggests that this field holds significant promise for the repair of jaw defects. The advantages of bone tissue engineering, notably its superior biocompatibility, exceptional mechanical properties, and biodegradability, position it as an exceptionally viable solution for addressing these complex medical challenges.[5,9,10]

Polylactic acid (PLA), known for its commendable biocompatibility and biodegradable byproducts of water and carbon dioxide, has been identified as an effective material for crafting composite porous scaffolds for bone tissue engineering. This revelation stands out as a significant advancement.[11] Nonetheless, its hydrophobic nature and associated challenges in cell adhesion somewhat limit its application in this field. Helal *et al.* demonstrated that augmenting PLA scaffolds with nano-hydroxyapatite (nHA) enhances surface roughness and increases cell adhesion sites, thereby facilitating osteogenic differentiation of stem cells for artificial bone tissue generation.[12] Furthermore, Wang *et al.* utilized fused deposition modeling (FDM) technology to fabricate nHA/PLA scaffolds, confirming their impressive biocompatibility, mechanical strength, and osteogenic induction capabilities.[13]

Infection during jaw repair poses a significant challenge for medical professionals. Chlorhexidine (CHX), a broad-spectrum antibacterial agent widely used in oral surgery, demonstrates extensive antibacterial activity, low cellular toxicity, and maintains its efficacy even in the presence of serum or blood. Consequently, CHX is regarded as an effective antibacterial

[a]*The Affiliated Hospital of Qingdao University, Qingdao, 266000, China. E-mail: sunjianqdfy@qdu.edu.cn; yanshan_l@qdu.edu.cn*

[b]*School of Stomatology, Qingdao University, Qingdao, 266000, China*

[c]*Dental Digital Medicine and 3D Printing Engineering Laboratory of Qingdao, Qingdao, 266000, China*

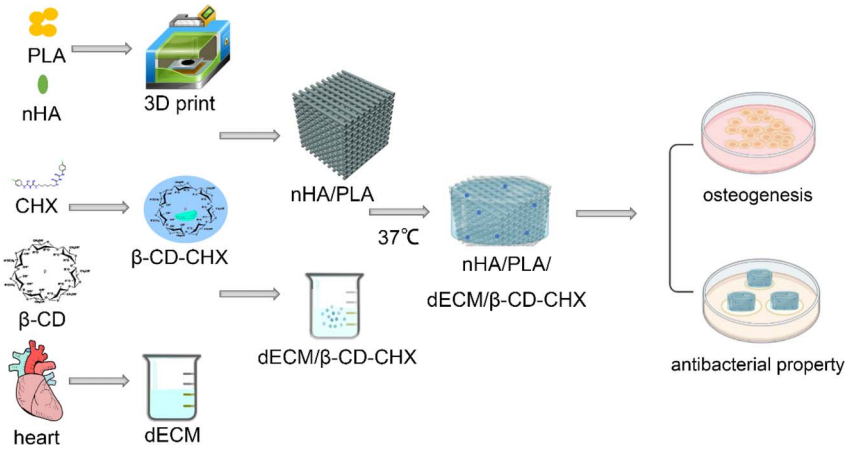


Fig. 1 Flow chart of nHA/PLA/dECM/β-CD–CHX preparation.

agent for treating jaw infections. However, issues arise with the premature release of a drug, which often compromises its antibacterial effectiveness.[14–16] To ensure a successful treatment outcome, drug delivery must be designed to provide long-term and effective antibacterial action at the surgical site, thereby preventing secondary infections due to premature antibiotic release. Existing research indicates that forming a β-CD inclusion complex with CHX results in a prolonged, sustained release without altering the drug's biocompatibility.[17]

In our quest for an effective carrier to deliver drugs for sustained antibacterial release at the targeted site, we turned our attention to the decellularized extracellular matrix (dECM). dECM hydrogels are derived from animal tissues subjected to decellularization treatments. Their remarkable biocompatibility, low immunogenicity, temperature-sensitive gelation, and their ability to promote cell proliferation and angiogenesis, along with a complexity difficult to replicate with synthetic materials, have garnered significant interest among clinical and scientific researchers.[18] dECM retains the native cellular structure and contains highly biologically active, non-antigenic components such as polysaccharides, collagen, glycoproteins, fibronectin, and integrins.[19,20] A key attribute of dECM is its preservation of numerous natural cell-binding sites, which are beneficial for cell adhesion, proliferation, and differentiation during bone regeneration. Decellularized extracellular matrix hydrogel scaffolds are currently extensively utilized in various fields, including full organ engineering for organ regeneration, bioprinting, tissue repair and reconstruction, disease modeling and drug screening, as well as in cell cultures.[21–23] In this study, we have innovatively incorporated dECM into the composite scaffold considering its temperature sensitive gel forming characteristics. This not only enables it to act as an effective drug carrier but also allows for the formation of a personalized hydrogel in the jaw defect area.

Consequently, this research encapsulated β-CD–CHX within the dECM and then integrated this dECM/β-CD–CHX complex onto an nHA/PLA scaffold, thereby fabricating a composite scaffold through temperature-sensitive gelation. The primary focus was to assess the osteogenic induction capabilities and antibacterial properties of this scaffold. To achieve these objectives, we conducted thorough examinations of the antibacterial efficiency and osteogenic induction potential of the nHA/PLA/dECM/β-CD–CHX scaffold, along with an in-depth analysis of its physical and chemical properties. The overarching aim of this study is to develop personalized bone tissue engineering scaffolds tailored to specific defect areas, thereby offering innovative solutions for clinical scenarios, particularly in repairing infected jaw defects (Fig. 1).

## 2. Experimental section

### 2.1. Materials

β-CD was acquired from Shanghai Boao Biotechnology Co., Ltd., while CHX was sourced from Sigma-Aldrich. We obtained nHA from Beijing DK Nano Technology Co., Ltd., and PLA was procured from Guoyao Chemical Reagent Co., Ltd. Additionally, the SDS solution was purchased from Shanghai Biyun Tian Biotechnology Co., Ltd., and Triton X-100 was supplied by Shanghai Aladdin Biochemical Technology Co., Ltd.

### 2.2. Preparation of β-CD–CHX

β-CD–CHX was prepared using the saturated aqueous solution method. First, 1.437 g of β-CD was dissolved in 20 ml of double-distilled water to obtain a saturated aqueous solution at 50 °C. Then, 0.64 g of CHX was dissolved in 10 ml of ethanol solution, with a molar ratio of CHX to β-CD set at 1 : 1. At 50 °C and under stirring, the CHX solution was introduced dropwise to the saturated aqueous solution of β-CD. After complete addition, stirring continued for 1 h and then the solution was cooled to 0–4 °C, left to stand overnight, filtered, washed, and concentrated.[17]

### 2.3. Preparation of composite hydrogel

Porcine left ventricular muscle tissue was selected, and the blood vessels and fat were removed. The tissue was cut into small pieces and repeatedly frozen and thawed three times at −80 °C. The decellularization process entailed soaking the muscle tissue in a 0.1% SDS solution for 24 hours with stirring and then treating it with a 1% SDS solution for an additional 48 hours, refreshing the solution at 24 hour intervals. The tissue was then

treated with 1% Triton X-100 for 1 hour and finally washed with deionized water. All solutions and instruments were strictly sterilized. dECM and myocardial tissue were stained with DAPI fluorescence to compare the cell nuclei removal effect.

The freeze-dried dECM was ground into powder and digested with pepsin in a pH = 2 solution for 24 hours. The pH was adjusted to 7.4 using a NaOH solution before mixing with β-CD–CHX. The mixture was stirred at room temperature for 2 hours before adding to the nHA/PLA scaffold using a temperature-sensitive gelation method. nHA/PLA/dECM/β-CD–CHX composite scaffolds were prepared.

### 2.4. Rheological properties of composite hydrogel

The dECM/β-CD–CHX at 4 °C was placed in a 1 ml volumetric flask and photographed again after heating to 37 °C.

The rheological properties of the dECM/β-CD–CHX were assessed using a rheometer (Physica MCR 92, Anton Paar, Germany). The storage modulus ($G'$) and loss modulus ($G''$) of dECM/β-CD–CHX were analyzed as a function of time at 37 °C.

### 2.5. Preparation of composite scaffold

Computer-aided design (CAD) software was employed to construct the three-dimensional shape of the scaffold, which included a 20 mm × 5 mm × 5 mm rectangular body and a cylinder measuring 10 mm in diameter and 5 mm in height. The internal pore size was set at 300 μm, with a line width of 30 μm. Polylactic acid (PLA) and nano-hydroxyapatite (nHA) were mixed in a 4 : 1 mass ratio and printed using a 3D printer. The printing conditions were carefully controlled: the temperature was maintained at (105 ± 5) °C, the printing bed temperature at 25 °C, the nozzle's movement speed at 6 mm $s^{-1}$, and the applied pressure at 350 kPa.

The nHA/PLA scaffold underwent a two-step disinfection process: initially, it was soaked in 75% ethanol for 1 hour, followed by ultraviolet radiation exposure for 2 hours. After being washed thrice with deionized water, the scaffold was immersed in the dECM/β-CD–CHX solution. To ensure deeper penetration of dECM/β-CD–CHX into the scaffold pores, vacuum assistance was employed. The temperature was gradually increased to 37 °C over 5 minutes and then sustained at 37 °C for 30 minutes to stabilize the composite scaffold. This study utilized these methodologies to prepare various scaffolds: the PLA scaffold (S1), nHA/PLA scaffold (S2), nHA/PLA/dECM scaffold (S3), and nHA/PLA/dECM/β-CD–CHX scaffold (S4).

### 2.6. Mechanical properties of composite scaffolds

The mechanical properties were tested with a tension-compression tester (Instron 5567, Instron, USA) at room temperature of 25 °C and humidity of 70%. Then, a compressive load was applied to the specimens, a cylindrical sample with a diameter of 10 mm and a height of 5 mm, at a strain rate of 1 mm $min^{-1}$ until each specimen was compressed to 80% of its initial height.[24]

From these analyses, we plotted stress–strain curves. The compressive strength was determined by the maximum value of the stress–strain curve, and the change of the composite hydrogel after addition to the scaffold was evaluated experimentally.[25] Three measurements were taken for each sample, and we used the mean to calculate the mean and standard deviation.

### 2.7. Drug release experiment

The absorption intensity of chlorhexidine (CHX) aqueous solution at 255 ± 2 nm was determined using a UV-visible spectrophotometer (Shimadzu, Japan) at concentrations of 2, 4, 6, 8, 10, 12, 16, 20, and 40 μg $ml^{-1}$. A standard curve for CHX was constructed using concentration and absorbance as the coordinates.

Precisely 0.5 g each of β-CD–CHX, composite hydrogel, and S4 were weighed and placed into dialysis bags. These bags were then immersed in 50 ml of PBS solution with a pH of 7.2, maintained at 37 °C, and stirred at a speed of 500 rpm. At predetermined intervals, 4 ml of the solution released from the bags was collected. The absorbance values of CHX in β-CD–CHX, dECM/β-CD–CHX composite hydrogels, and S4 composite scaffolds were recorded at various time points. The PBS solution was replenished as necessary. After a period of 5 weeks, the total drug release rate was quantified. The amount of drug released was calculated using the standard curve equation.

The drug release rate was determined using the formula: (drug release quantity/sample drug quantity) × 100%. This experiment was conducted in triplicate to ensure accuracy, and the average value and standard deviation were calculated.

### 2.8. Cell proliferation experiment

The S1 and S2 scaffolds are disinfected by soaking in 75% ethanol for 1 hour, and then subjected to UV irradiation for 2 hours. dECM, dECM/β-CD–CHX are combined to construct the S1, S2, S3, and S4 scaffold groups. The scaffolds are washed three times with deionized water. Each scaffold group is placed in a 37 °C and 5% $CO_2$ cell culture incubator and immersed in Dulbecco's modified Eagle's medium (DMEM) containing 10% fetal bovine serum and 1% penicillin/streptomycin (ISO 10993-part 12). After 72 hours, the extracts are collected and stored at 4 °C.

MC3T3-E1 cells (ATCC, CRL-2594) in the logarithmic phase are obtained and adjusted to a concentration of $5 \times 10^4$ $ml^{-1}$. To a 96-well plate, 100 μl of cell culture fluid is added. The experiment is organized into a control group and S1, S2, S3, S4 groups. At 1, 3, and 5 day intervals, 10 μl of CCK-8 solution is added and incubated at 37 °C for 1 hour. The absorption wavelength at 450 nm is read using an enzyme-linked immunosorbent assay reader. Cell proliferation is assessed through live/dead cell staining, followed by observation under a fluorescence microscope (Olympus IX 51, Japan). This experiment is conducted in triplicate with independent duplications.

### 2.9. Cell adhesion experiment

S1, S2, S3, and S4 scaffolds are placed in 24-well plates and inoculated with MC3T3-E1 cells ($5 \times 10^4$ cells per well), cultured for 24 hours for cell adhesion. The scaffolds are then washed with PBS (pH = 7.4), fixed in glutaraldehyde at 4 °C for 2 hours, rinsed, and dehydrated with graded alcohols. After critical point drying and gold spraying, they are analyzed by SEM. This experiment is conducted thrice with independent duplications.

### 2.10. Osteogenic experiment

Each group of scaffolds is soaked in a culture medium containing 10% fetal bovine serum and 1% penicillin–streptomycin. MC3T3-E1 cells are co-cultivated with each group of medium, inoculated at $2 \times 10^4$ cells per well in a 12-well plate. Once the cells reach 80% confluence, 100 nmol $l^{-1}$ dexamethasone, 50 μg $ml^{-1}$ ascorbic acid, and 10 mmol $l^{-1}$ β-glycerophosphate are added to induce osteogenic differentiation. The osteogenic induction medium is replaced every 2 days. The osteogenic differentiation ability of the S1, S2, S3, and S4 groups is evaluated through ALP staining and alizarin red staining.

ALP activity and staining were assessed using an alkaline phosphatase (ALP) assay kit (Nanjing Jiancheng Bioengineering Research Institute Co. LTD) and an ALP staining kit (Dalian Boglin Biotechnology Co. LTD) on days 7 and 14. On day 21, cells were fixed with 4% paraformaldehyde for 30 minutes, followed by three washes with PBS. They were then stained with a 2% alizarin red solution (Dalian Meilun Biotechnology Institute) for 45 minutes. Calcium nodules were

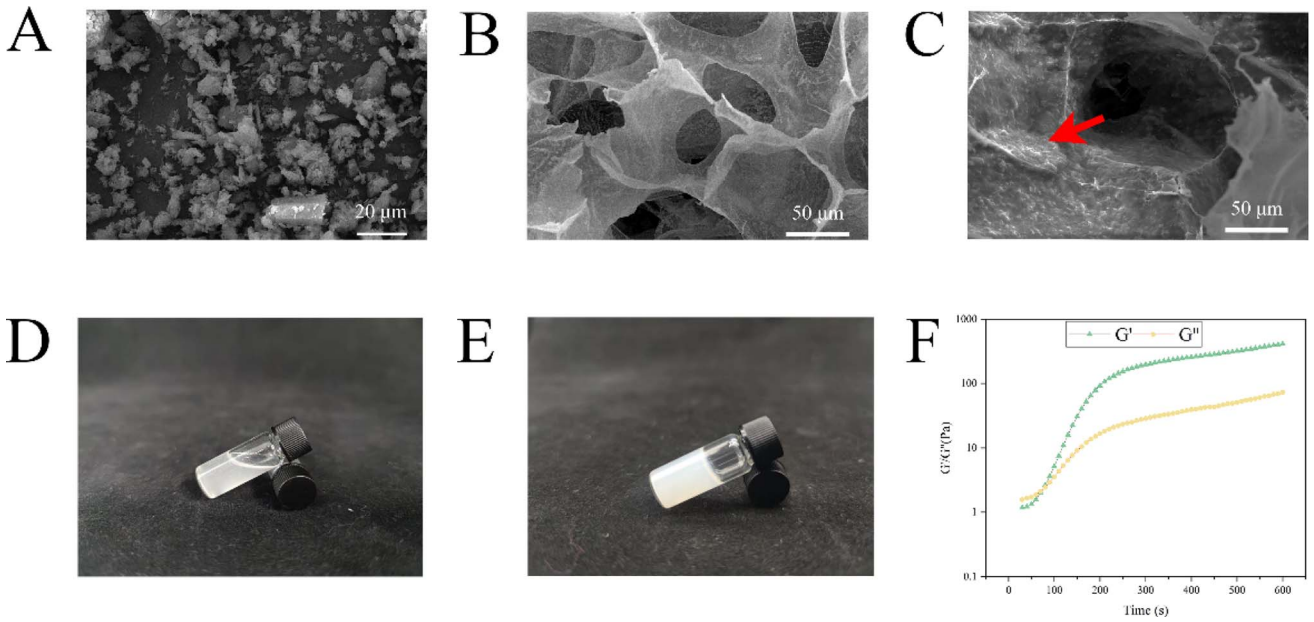


Fig. 2 Representative SEM images: β-CD–CHX 2000× (A). dECM 1000× (B). dECM/β-CD–CHX 1000× (C). dECM/β-CD–CHX at 4 °C (D). dECM/β-CD–CHX at 37 °C (E). Elastic modulus of dECM/β-CD–CHX at 37 °C (F).

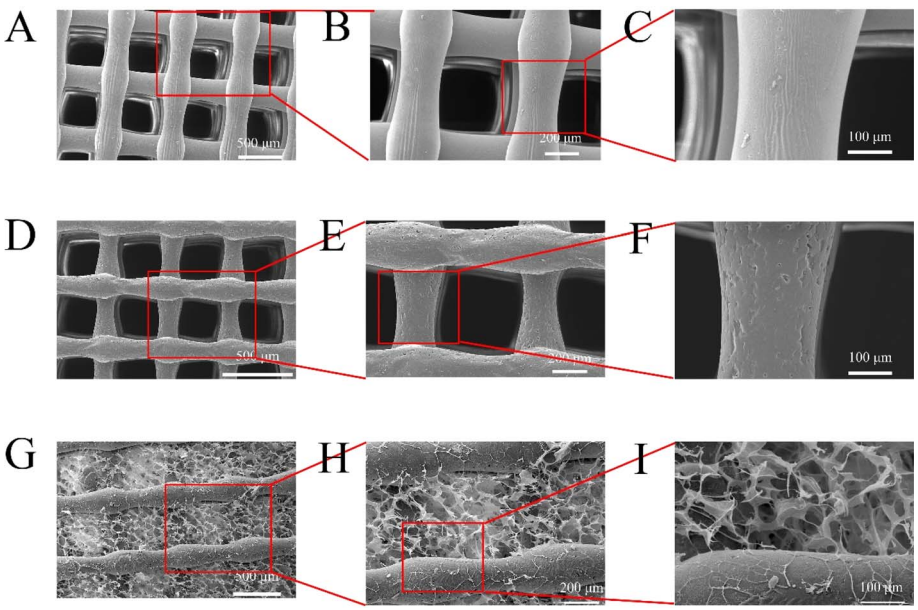


Fig. 3 Representative SEM images: S1 (A–C). S2 (D–F). S4 (G–I). (A, D and G) 100×, (B, E and H) 200×, and (C, F and I) 500×.

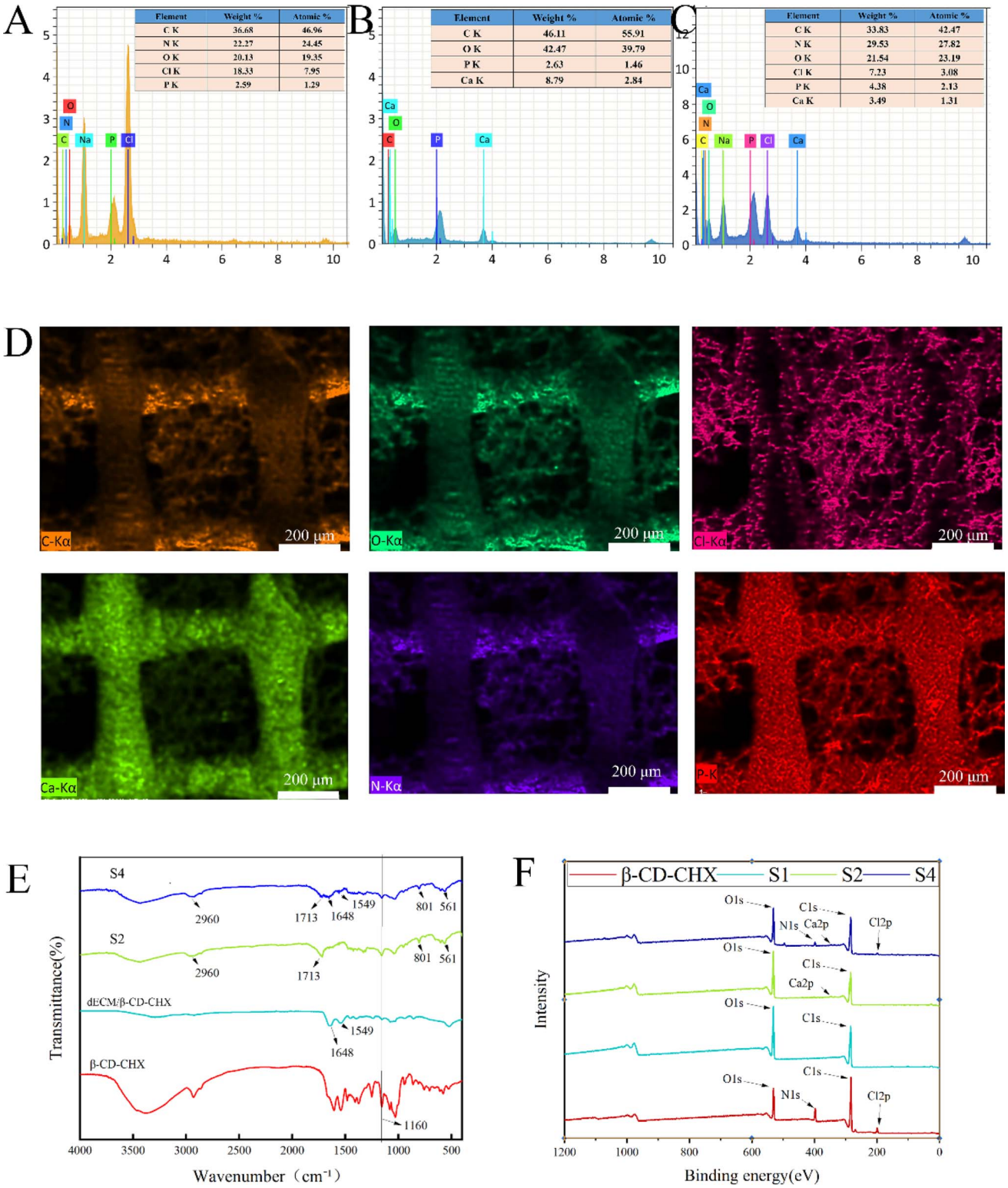


Fig. 4 Scaffold characterization: elemental composition of β-CD–CHX (A). Elemental composition of S2 (B). Element composition of S4 (C). Elemental distribution of S4 (D). FTIR (E). XPS (F).

observed under a light microscope, and acetylpyridine chloride was used for the alizarin red qualitative test. These experiments were performed in triplicate and independently repeated three times.

### 2.11. Antimicrobial experiment

The experiments were divided into five groups: a control group and the S1, S2, S3, and S4 scaffold groups. These scaffolds were incubated in culture medium for 72 hours. *Staphylococcus*

*aureus* (ATCC 6538) and *Escherichia coli* (ATCC 8739) were mixed with the extract to create a 0.5 McFarland standard bacterial suspension. The antibacterial activities of the 3D-printed scaffolds against these bacteria were tested using the agar plate method. First, 20 μl of agar culture medium was poured into culture dishes to solidify. Next, 100 μl of inoculum was added and evenly distributed over the agar. The control, S1, S2, S3, and S4 scaffolds were placed on the agar plates and incubated at 37 °C for 24 hours to form inhibition zones. Photographs were taken to document the results. This procedure was repeated three times independently.

Additionally, the antibacterial abilities of the scaffolds were verified by bacterial colony counting. The bacterial solution was diluted to different concentrations, and OD values were measured to select the appropriate dilution factor. The co-culture medium, diluted accordingly, was incubated at 37 °C for 24 hours, further diluted to $10^{-6}$ and 20 μl of this solution was spread onto plates. After another 24 hour incubation at 37 °C, colony counts were calculated, and photographs recorded the results. This part of the experiment was also performed in triplicate and independently repeated three times.

### 2.12. Data analysis

All data sets were subjected to statistical analysis using Origin Pro 9.0 software (Origin Lab, Massachusetts, USA). The single factor analysis of variance was employed for the comparisons. $^{*}P < 0.05$ was considered to be statistically significant.

## 3. Results and discussion

### 3.1. Preparation and characterization of composite hydrogel

Utilizing scanning electron microscopy (SEM), the study observed the morphologies and microstructures of β-CD–CHX, dECM, and dECM/β-CD–CHX composite hydrogels. The synthesized β-CD–CHX demonstrated a needle-like structure (Fig. 2A). The dECM, in contrast, presented a porous structure (Fig. 2B). Notably, the porosity of the dECM hydrogel exceeded 60%, a determination made using ImageJ software.[26] This porous architecture is instrumental in facilitating nutrient exchange and enhancing cell adhesion and proliferation.

β-CD–CHX was successfully bound to dECM, resulting in a rough surface on the hydrogel without affecting the porous structure of dECM. Needle-like β-CD–CHX was observed on the surface of the hydrogel (Fig. 2C).

We subjected the dECM to 4 °C and 37 °C to verify its temperature-sensitive properties, and the results showed that the dECM was a liquid at 4 °C and solid at 37 °C (Fig. 2D and E). The elastic modulus of the dECM hydrogel was measured at 37 °C. $G'$ exceeded $G''$ at about 80 s, indicating the presence of cross-links in the dECM hydrogel (Fig. 2F), and $G'/G''$ gradually increased with time, indicating that the hardness and gel strength of the composite hydrogel increased.[27] However, the $G'/G''$ did not change significantly after 300 s, indicating that the composite hydrogel reaction was basically completed.

### 3.2. Preparation and characterization of composite scaffold

SEM showed that the pores of S1, S2, and S4 scaffolds were uniform, with a diameter of 250 μm and a spacing of about 300 μm. Fig. 3A shows that the surface of a single S1 is smoother than that of S2 and S4.

Consistent with prior research,[28] the surface of the S2 scaffold acquired a rougher texture upon introducing nano-hydroxyapatite (nHA) (Fig. 3F). Moreover, the incorporation of nHA and composite hydrogels resulted in an augmented surface area of the scaffold while preserving the porous attributes of dECM hydrogels (Fig. 3I). Such a feature offers an enhanced substrate for cell adhesion. When implanted into the jaw bone, the composite scaffold not only provides a conducive environment for osteoblast proliferation but also aids in bone regeneration.[29]

Energy-dispersive X-ray spectroscopy (EDS) analysis revealed the elemental composition of β-CD–CHX (Fig. 4A) as C, N, O, Cl, and P. The S2 scaffold (Fig. 4B) comprised elements such as C, O, P, and Ca, while the S4 scaffold (Fig. 4C) contained C, N, O, Cl, P, and Ca. The presence of these elements affirmed the successful printing of the S4 scaffold. Mapping analysis (Fig. 4D) further corroborated the uniform distribution of these elements within the scaffold.

In FTIR analysis (Fig. 4E), the S2 scaffold demonstrates distinct spectral characteristics: a peak at 2960 $cm^{-1}$, which is associated with C–H bending, and another prominent peak at

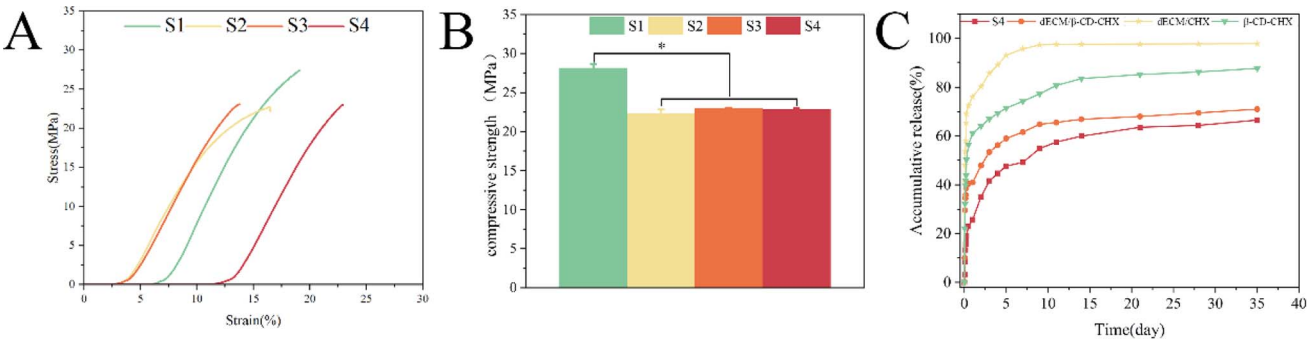


Fig. 5 Compressive mechanical properties of scaffolds: stress–strain curve (A). Compressive strength (B) and *in vitro* release profiles of β-CD–CHX, dECM/CHX, dECM/β-CD–CHX, and S4 (C).

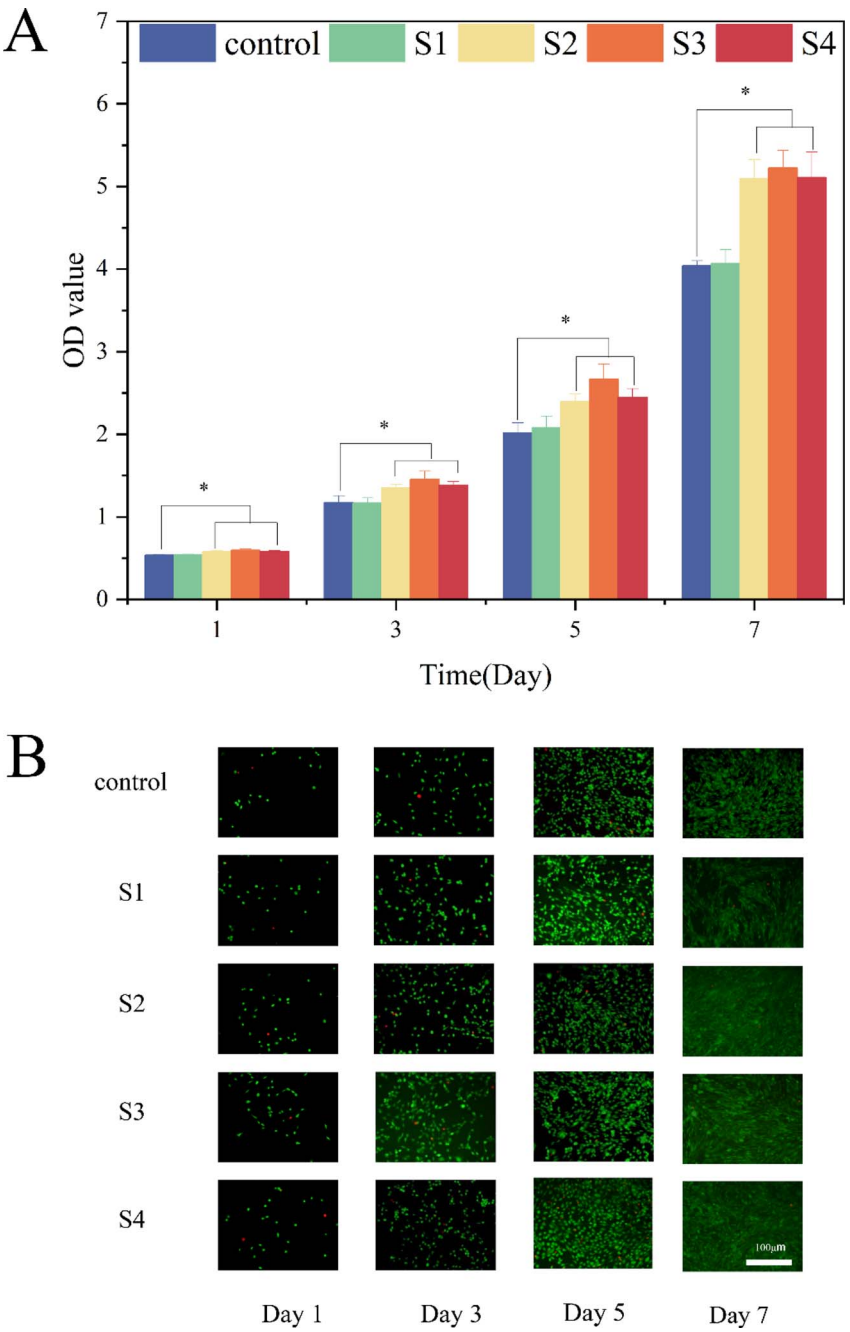


Fig. 6 Cell compatibility: the CCK-8 method was used to detect the proliferation of MC3T3-E1 cells cultured in control, S1, S2, S3, S4 groups for 1, 3, 5 and 7 days (A). Live and dead cell staining (B).

1713 $cm^{-1}$ corresponding to the stretching of C=O groups. Additionally, a peak at 801 $cm^{-1}$ indicates the stretching vibration of C–H. The characteristic peak of nHA at 561 $cm^{-1}$, associated with the –OH group,[28] aligns with previous findings. The β-CD–CHX spectrum, shown in Fig. 4E, exhibits a characteristic peak at 1160 $cm^{-1}$, attributed to C–O stretching vibrations.[30] In the dECM spectrum (Fig. 4E), a peak at 1648 $cm^{-1}$ correlates with amide I type vibrations, and another at 1549 $cm^{-1}$ is linked to C=O stretching vibrations and N–H bending in peptides.[31,32] The presence of these peaks in the composite scaffold's spectrum confirms the successful printing of the multi-porous scaffold.

The XPS analysis reveals that the S4 scaffold primarily comprises C, N, O, Cl, Ca, and P elements, corroborating the elemental analysis results (Fig. 4F). Compared to S2, S4 exhibits distinct peaks at N 1s and Cl 2p in its XPS spectrum. The C/O ratio of S1 is relatively high at 1.93, but it decreases to 1.19 for S2 and further to 1.04 for S4 following the addition of nHA and composite hydrogel. This shift suggests that the inclusion of more oxygen atoms modifies the chemical composition of the

 

S1 surface,[30,33] thus affirming the successful printing of the S4 composite porous scaffold. Additionally, the composition and structure of S2 remain unchanged after the drug's addition, corroborating the findings from the FTIR analysis.

### 3.3. Mechanical properties of composite scaffolds

The mechanical analysis of the composite scaffolds in each group was carried out by compression experiments. Fig. 5A shows the stress–strain curves of S1, S2, S3, and S4 scaffolds, through which the compressive strength of each scaffold was obtained (Fig. 5B). The compressive strengths of S1, S2, S3 and S4 were (28.14 ± 0.55 MPa), (22.30 ± 0.55) MPa, (22.93 ± 0.14) MPa and (22.83 ± 0.17) MPa, respectively. The average compressive strength of S1 was higher than that of S2, S3, and S4 ($p < 0.05$), which was related to the weakened mechanical properties of the scaffold after the addition of nHA. There was no significant difference between S2, S3 and S4, but the compressive strength of S3 and S4 was slightly higher than that of S2, which may be related to the hydrogel filling in the gap of the scaffold. However, this difference is not clinically significant and composite scaffolds can fully meet the mechanical properties of human bone.[34]

### 3.4. Drug release experiment

During the first week on the S4 surface, CHX was predominantly released, resulting in a rapid release rate from the composite porous scaffold (Fig. 5C). Subsequently, the release rate transitioned to a sustained phase due to the dual lag effect of dECM and β-CD–CHX. It was observed that the drug release rate of S4 reached 60% in the first month, in contrast to the 87% release from β-CD–CHX. As CHX was released in large quantities from β-CD–CHX, S4 underwent gradual degradation, leading to a consistent release curve without a sudden or interrupted release. This pattern indicates an even distribution of β-CD–CHX in S4, ensuring a sustained release of CHX. After 35 days, 66% drug release was achieved due to the sustained release properties of the composite scaffold, and CHX could continue to be released from S4. The release of dECM/CHX reached 97% on the 7$^{th}$ day, which may be because the loose and porous hydrogel alone cannot achieve a better sustained release effect. However, 87% and 71% of β-CD–CHX and dECM/β-CD–CHX were released after 35 days. This is critical considering the ongoing risk of jawbone infection before complete healing. The combined effects of S2, dECM, and β-CD–CHX facilitate a long-term release of CHX, playing a crucial anti-infective role in treating jawbone defects, highlighting its significance as a bone substitute in infectious jaw defect repair.[35]

### 3.5. Cell proliferation experiment

The cell proliferation was assessed using the Cell Counting Kit-8 (CCK-8) on days 1, 3, 5 and 7. The results revealed that the cell counts for the S2, S3, and S4 groups were significantly higher than those of the S1 and control groups ($P < 0.05$), indicating their superior potential for cell proliferation (Fig. 6A). Notably, the optical density (OD) values between the S2 and S4 groups showed no significant differences, suggesting that the incorporation of dECM and β-CD–CHX did not adversely impact cell viability. In addition, MC3T3-E1 cells exhibited higher density on the S2 and S4 scaffolds, aligning with previous studies.[36] As shown in Fig. 6A, S3 demonstrated a more robust proliferation effect than S2, though the influence of dECM on cell proliferation was not statistically significant. This might be attributed to the slightly shorter duration of cell culture. Also, the addition of dECM and sustained-release drugs did not heighten the cytotoxicity of S4.[30,37]

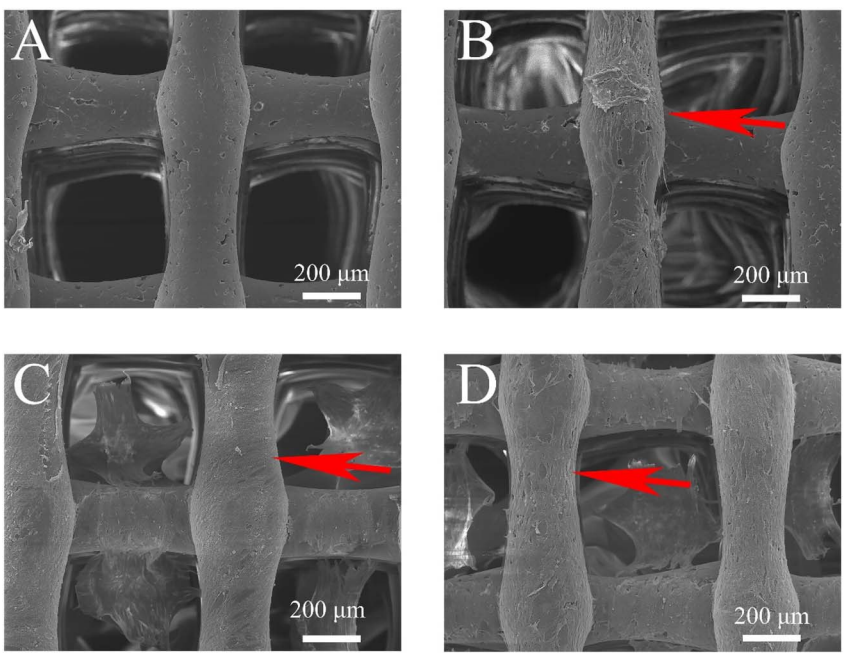


Fig. 7 SEM images of MC3T3-E1 adhering to S1 (A). S2 (B). S3 (C). S4 (D).

Further analysis with live/dead staining (Fig. 6B), conducted after 1, 3, 5 and 7 days of cultivation, showed that MC3T3-E1 cells remained healthy, corroborating the suitability of S4 as a substrate for live cell adhesion. The integration of nHA into the S1 scaffold enhanced the diffusion and proliferation of MC3T3-E1 cells.[38] Moreover, S4 retained good biocompatibility even after adding dECM/β-CD–CHX.

These findings collectively indicate that S4 possesses excellent cytocompatibility, making it a promising candidate as a bone implant material for the repair of jaw defects.

### 3.6. Cell adhesion experiment

The cell adhesion assay revealed that MC3T3-E1 cells could firmly adhere to and proliferate around the scaffold after 24 hours of culture. SEM analysis indicated that cells on S2 (Fig. 7B), S3 (Fig. 7C), and S4 (Fig. 7D) showed more extensive proliferation and adherence to the scaffold and hydrogel surface compared to S1 (Fig. 7A). S3 and S4 demonstrated superior adhesion, with pseudopodia fully extended and fusiform in shape, compared to S1 and S2. This enhanced adhesion is likely due to the composite scaffold's rougher surface and increased surface area, afforded by the addition of nHA and dECM, which provide more sites for cells.[21,22,38]

### 3.7. Osteogenesis experiment

ALP staining (Fig. 8A) and quantitative analysis (Fig. 8C) were conducted on MC3T3-E1 cells from each group on days 7 and 14. Compared to the S1 and control groups, the ALP staining of

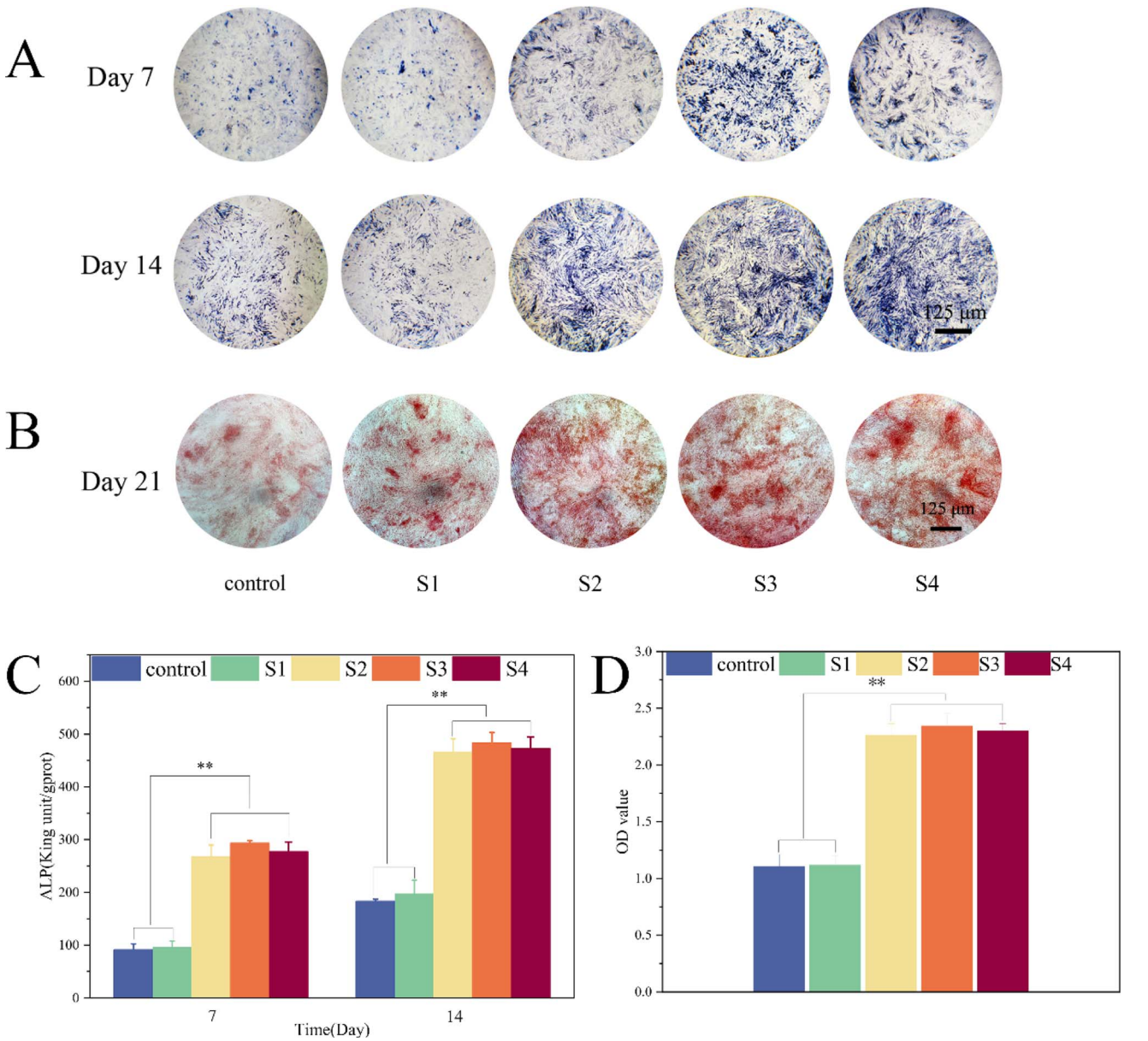


Fig. 8 MC3T3-E1 cell osteogenic assay: ALP qualitative and quantitative experiments at 7 and 14 days. (A and C). Qualitative and quantitative experiments with alizarin red at 21 days (B and D).

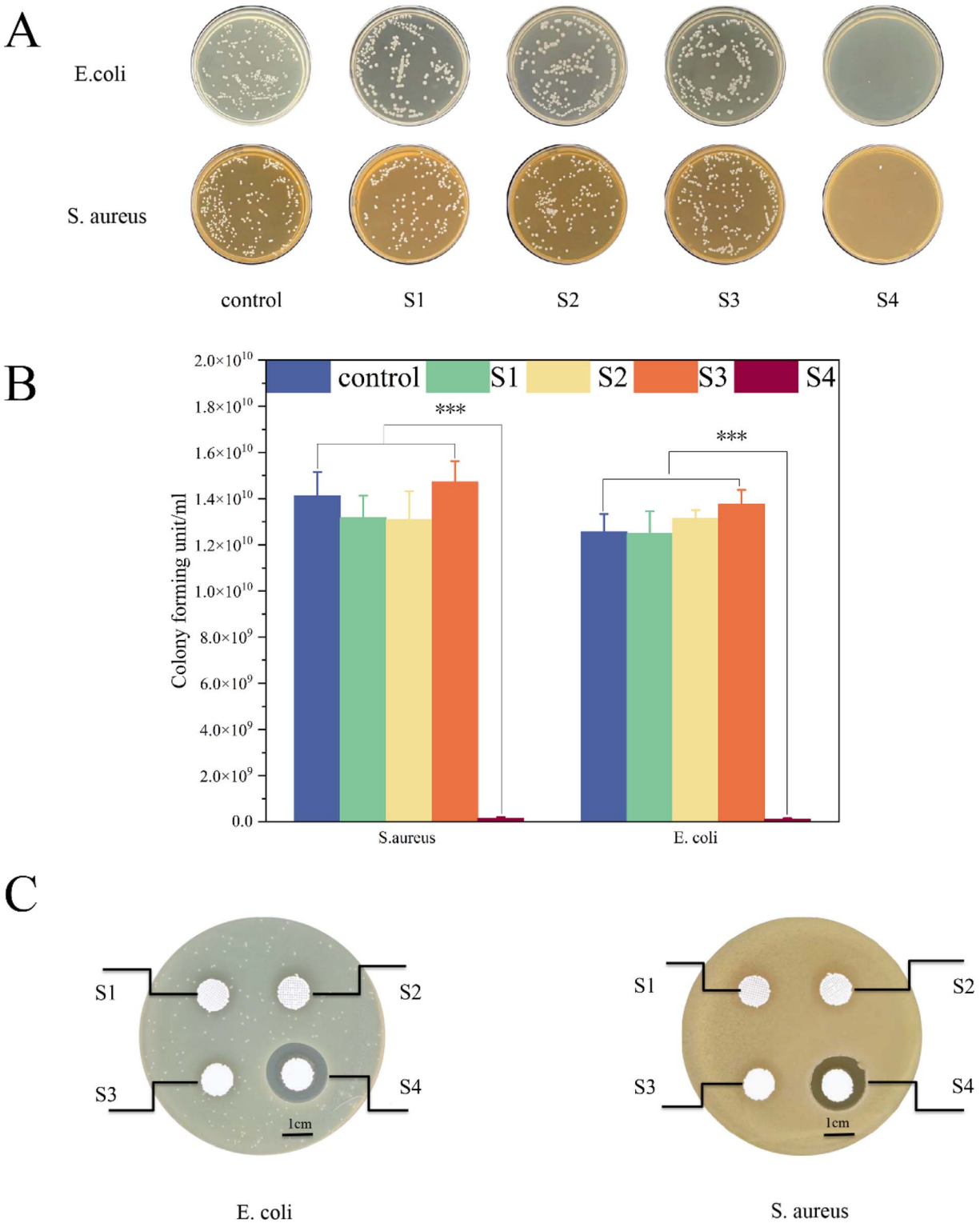


Fig. 9 Bacterial experiments: photos of CFU experiments (A). CFU quantification experiments (B). Inhibition ring test (C).

the S2, S3, and S4 groups showed a marked increase (Fig. 8A). The quantitative analysis of ALP activity, as depicted in Fig. 8C, indicated that the ALP activity in S4 was significantly higher than that in the S1 and control groups ($P < 0.01$). Furthermore, there were no significant differences in ALP activity among the S2, S3, and S4 groups ($P > 0.05$). This suggests that the incorporation of dECM not only increased cell adhesion sites but also promoted cell proliferation and enhanced bone tissue regeneration. These results align with the findings of Pati *et al.*, who observed that dECM-modified scaffolds facilitated increased mineralized tissue formation and bone regeneration at both ectopic and orthotopic sites.[21,22] The addition of dECM

to S4 enhanced cell proliferation without compromising its osteogenic performance. After 21 days of cultivation, alizarin red staining (Fig. 8B) and subsequent quantitative analysis (Fig. 8D) were performed on the control group, and S1, S2, S3, and S4 groups. Alizarin red staining (Fig. 8B) revealed that after 21 days of osteogenic induction, mineralized nodules were present in all groups. The S2, S3, and S4 groups exhibited a higher quantity of calcium deposits compared to the control and S1 groups. The quantitative analysis and calcium nodule staining (Fig. 8D) were consistent, indicating that S4 had a superior capacity for inducing osteoblast differentiation. dECM-modified scaffolds have been recognized for their osteoinductive and osteoconductive properties.[21] Additionally, nHA is known for its osteoinductive characteristics and high affinity for bone tissue, rendering it an ideal polymer scaffold for bone regeneration that can mimic natural bone tissue.[12] The efficacy of S4 in inducing osteogenic differentiation was further validated through osteogenic induction experiments.

### 3.8. Antimicrobial experiment

After co-culturing with *Escherichia coli* and *Staphylococcus aureus* for 24 h, each group was counted by Colony-Forming Units (CFU) (Fig. 9A and B). The colony count for the S4 group was notably lower than that of the S1, S2, and S3 groups ($P < 0.001$), indicating the significant antibacterial properties of the sustained-release drug. As shown in Fig. 9C, an inhibitory zone with a diameter of 1 cm was evident in the S4 region. This result confirms the effectiveness of integrating CHX into the S4 scaffold against both *Staphylococcus aureus* and *Escherichia coli*. CHX is a well-established antimicrobial agent in hygiene and is particularly valuable as an antibacterial agent in oral medicine where mechanical prevention is not feasible.[39] The addition of CHX to the scaffold prevents the adherence and proliferation of *Staphylococcus aureus* and *Escherichia coli*, playing a key role in preventing infections in jawbone defects.[40]

## 4. Conclusion

In conclusion, this study successfully synthesized an osteogenic and antibacterial composite scaffold. The surface morphology of the scaffold, as analyzed by scanning electron microscopy, revealed a uniform structure with rough and porous surfaces, which are conducive to cell adhesion and proliferation. The characterization studies corroborated that the composite hydrogel and the sustained-release drug were uniformly dispersed within the composite scaffold. The drug release experiments demonstrated that the antibacterial drug could be released in a stable and continuous manner from the composite scaffold over an extended period. Furthermore, the composite scaffold exhibited excellent biocompatibility, enhancing cell proliferation, inducing osteogenic differentiation in osteoblasts, and promoting the formation and regeneration of bone tissue. The efficacy of the scaffold's antibacterial properties was confirmed through CFU and antibacterial ring experiments. Overall, the 3D-printed composite porous scaffold provides a tailored solution for the clinical repair of large-area infectious jawbone defects, showcasing its potential in regenerative medicine and implantology.

## Author contributions

Conceptualization, Z. L. and L. C.; writing – original draft preparation, X. G. and Y. D.; writing – review and editing, Z. X. and L. L.; suggestions on revision, L. C. and Y. L.; funding acquisition, J. S. All authors have read and agreed to the published version of the manuscript. All authors have contributed substantially to the work reported.

## Conflicts of interest

There are no conflicts to declare.

## Acknowledgements

The author(s) declare financial support was received for the research, authorship, and/or publication of this article. This research was funded by the Qingdao Medical and Health Research Program (grant number: 2021-WJZD193), the Qingdao University Affiliated Hospital Clinical Medicine + X Scientific Research Project (grant number: QDFY+X202101041 and QDFY+X2023207), the Shandong Province Medical and Health Technology Development Plan Project (grant number: 202208020979 and 202308020875), Science and Technology Project of Qingdao city south District (grant number: 2023-2-005-YY), Oral Medicine Climbing Discipline Project in Qingdao.

## Notes and references

1 D. R. J. Millard, *Plast. Reconstr. Surg.*, 1965, **35**, 60–75.
2 I. R. Reid and J. Cornish, *Nat. Rev. Rheumatol.*, 2012, **8**, 90–96.
3 M. F. M. Guerra, L. N. Gías, F. R. g. Campo and J. S. Pérez, *J. Oral Maxillofac. Surg.*, 2003, **61**, 1289–1296.
4 D. Posw1llo, *Development*, 1988, **103**, 207–212.
5 S. Basyuni, A. Ferro, V. Santhanam, M. Birch and A. McCaskie, *Br. J. Oral Maxillofac. Surg.*, 2020, **58**, 632–642.
6 M. Martola, C. Lindqvist, H. Hänninen and J. Al-Sukhun, *J. Biomed. Mater. Res., Part B*, 2007, **80**, 345–352.
7 M. Batstone, *Aust. Dent. J.*, 2018, **63**, S108–S113.
8 D. L. Master, P. R. Hanson and A. K. Gosain, *J. Craniofac. Surg.*, 2010, **21**, 1565–1570.
9 S. Konopnicki and M. J. Troulis, *J. Oral Maxillofac. Surg.*, 2015, **73**, S136–S146.
10 H. E. Jazayeri, M. Tahriri, M. Razavi, K. Khoshroo, F. Fahimipour, E. Dashtimoghadam, L. Almeida and L. Tayebi, *Mater. Sci. Eng. Carbon*, 2017, **70**, 913–929.
11 I. Armentano, N. Bitinis, E. Fortunati, S. Mattioli, N. Rescignano, R. Verdejo, M. A. López-Manchado and J. M. Kenny, *Prog. Polym. Sci.*, 2013, **38**, 1720–1747.
12 M. H. Helal, H. D. Hendawy, R. A. Gaber, N. R. Helal and M. N. Aboushelib, *J. Prosthet. Dent.*, 2019, **121**, 118–123.
13 W. Wang, B. Zhang, M. Li, J. Li, C. Zhang, Y. Han, L. Wang, K. Wang, C. Zhou and L. Liu, *Composites, Part B*, 2021, **224**, 109192.

14 A. Russell and M. Day, *J. Hosp. Infect.*, 1993, **25**, 229–238.
15 T. Kuyyakanond and L. B. Quesnel, *FEMS Microbiol. Lett.*, 1992, **100**, 211–215.
16 C. A. Soriano-Souza, A. L. Rossi, E. Mavropoulos, M. A. Hausen, M. N. Tanaka, M. D. Calasans-Maia, J. M. Granjeiro, M. H. M. Rocha-Leão and A. M. Rossi, *J. Mater. Sci.: Mater. Med.*, 2015, **26**, 1–15.
17 L. Cheng, Z. Xu, Y. Li, D. Zhou, L. Chen, Y. Liu, Y. Xu, K. Meng and J. Sun, *Mater. Lett.*, 2022, **309**, 131460.
18 L. T. Saldin, M. C. Cramer, S. S. Velankar, L. J. White and S. F. Badylak, *Acta Biomater.*, 2017, **49**, 1–15.
19 A. D. Theocharis, S. S. Skandalis, C. Gialeli and N. K. Karamanos, *Adv. Drug Delivery Rev.*, 2016, **97**, 4–27.
20 E. D. Hay, *Cell Biology of Extracellular Matrix*, Springer Science & Business Media, 1991.
21 F. Pati, T.-H. Song, G. Rijal, J. Jang, S. W. Kim and D.-W. Cho, *Biomaterials*, 2015, **37**, 230–241.
22 J. Zhang, E. Wehrle, P. Adamek, G. R. Paul, X.-H. Qin, M. Rubert and R. Müller, *Acta Biomater.*, 2020, **114**, 307–322.
23 C. E. Pedraza, B. Marelli, F. Chicatun, M. D. McKee and S. N. Nazhat, *Tissue Eng., Part A*, 2010, **16**, 781–793.
24 S. L. Marshall, T. D. Jacobsen, E. Emsbo, A. Murali, K. Anton, J. Z. Liu, H. H. Lu and N. O. Chahine, *ACS Biomater. Sci. Eng.*, 2021, **7**, 5836–5849.
25 R. L. Keate, J. Tropp, C. Serna and J. Rivnay, *Cell. Mol. Bioeng.*, 2021, **14**, 501–512.
26 S. L. Goodman, P. A. Sims and R. M. Albrecht, *Biomaterials*, 1996, **17**, 2087–2095.
27 Y. Yu, H. Jin, L. Li, X. Zhang, C. Zheng, X. Gao, Y. Yang and B. Sun, *J. Nanobiotechnol.*, 2023, **21**, 308.
28 Y. Zheng, G. Fu, B. Wang, C. Pang, P. Hall and N. Sharmin, *J. Appl. Polym. Sci.*, 2020, **137**, 49286.
29 S. Wu, X. Liu, K. W. Yeung, C. Liu and X. Yang, *Mater. Sci. Eng., R*, 2014, **80**, 1–36.
30 L. Cheng, Z. Xu, Y. Liu, D. Zhou, M. Sun, Y. Xu, L. Chen and J. Sun, *ACS Appl. Polym. Mater.*, 2022, **4**, 4476–4485.
31 R. Cheheltani, C. M. McGoverin, J. Rao, D. A. Vorp, M. F. Kiani and N. Pleshko, *Analyst*, 2014, **139**, 3039–3047.
32 K.-Z. Liu, M. Jackson, M. G. Sowa, H. Ju, I. M. Dixon and H. H. Mantsch, *Biochim. Biophys. Acta, Mol. Basis Dis.*, 1996, **1315**, 73–77.
33 H. E. Canavan, D. J. Graham, X. Cheng, B. D. Ratner and D. G. Castner, *Langmuir*, 2007, **23**, 50–56.
34 X. Gao, Z. Xu, S. Li, L. Cheng, D. Xu, L. Li, L. Chen, Y. Xu, Z. Liu and Y. Liu, *RSC Adv.*, 2023, **13**, 3759–3765.
35 Y. Yang, L. Chu, S. Yang, H. Zhang, L. Qin, O. Guillaume, D. Eglin, R. G. Richards and T. Tang, *Acta Biomater.*, 2018, **79**, 265–275.
36 X. Li, Y. Wang, Z. Wang, Y. Qi, L. Li, P. Zhang, X. Chen and Y. Huang, *Macromol. Biosci.*, 2018, **18**, 1800068.
37 B. Wu, L. Jin, K. Ding, Y. Zhou, L. Yang, Y. Lei, Y. Guo and Y. Wang, *J. Mater. Chem. B*, 2020, **8**, 10616–10629.
38 M.-E. Grigora, Z. Terzopoulou, D. Baciu, T. Steriotis, G. Charalambopoulou, E. Gounari, D. N. Bikiaris and D. Tzetzis, *J. Mater. Sci.*, 2023, **58**, 2740–2763.
39 F. P. Deus and A. Ouanounou, *Int. Dent. J.*, 2022, **72**, 269–277.
40 Z. L. Brookes, R. Bescos, L. A. Belfield, K. Ali and A. Roberts, *J. Dent.*, 2020, **103**, 103497.